ACS Sustainable Chemistry & Engineering

pubs.acs.org/journal/ascecg

Research Article

Engineering Lignin Nanoparticles: A Tandem Fractionation and Enzymatic Oxidation Approach to Control Size and Hydrophobicity

Nicolò Pajer, Valerio C. A. Ficca, Ernesto Placidi, Dimitris S. Argyropoulos, Matteo Gigli,* and Claudia Crestini

Cite This: *ACS Sustainable Chem. Eng.* 2026, 14, 8233−8243

Read Online

ACCESS | Metrics & More | Article Recommendations | Supporting Information

ABSTRACT: Lignin nanoparticles (LNPs) are pivotal for the advancement of modern and sustainable biorefineries. Yet, optimizing their performance requires precise control over size and hydrophobicity. This study investigates a tandem approach involving fractionation and laccase-mediated oxidation of hardwood kraft lignin prior to nanosizing. Two solvent precipitation methods for LNP synthesis are compared: a sodium tosylate system (yielding hLNPs) and an ethanol:water mixture (yielding eLNPs). Results indicate that biocatalytic modifications, primarily the reduction of hydroxyl groups and increased molecular weight through radical coupling, are key determinants of the yield, dimensions, and surface functionalities of the resulting LNPs. These properties are governed by an interplay of chain-folding capability, supramolecular interactions, and specific solvation mechanisms. Notably, hLNPs exhibit diameters of 500−750 nm, whereas eLNPs are significantly smaller (<230 nm). Lastly, XPS analysis confirms successful hydrophobization, revealing up to a 45% reduction in surface hydroxyl functionalities and a 2.6-fold increase in ketone groups compared to pristine counterparts. This research provides a robust and eco-friendly strategy for engineering tailored LNPs with enhanced applicability potential.

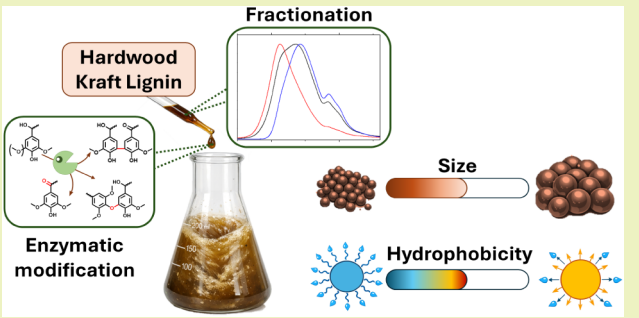

KEYWORDS: *lignin nanoparticles, lignin fractionation, laccase, biocatalytic process, oxidative treatment, solvent precipitation, hydrotropic process, lignin hydrophobization*

INTRODUCTION

More than 30% of the plant biomass mass is composed of lignin, the most abundant aromatic biopolymer.[1] The annual production of technical lignins is estimated at 100 million tonnes/year,[2] primarily isolated as a byproduct of pulping industries (kraft, soda, and lignosulfonates) and modern biorefineries (organosolv). Unfortunately, despite its abundance, there are no high-value applications for a full integration of lignin in circular systems. Efforts to efficiently valorize lignin have been recently pursued exploring the isolation of high-value products (like pyrolysis oil or benzene, toluene, and xylenes)[3,4] and the production of materials (such as phenolic resins, polyurethanes, and vitrimers).[5,6] However, a critical analysis of the status of lignin valorization reveals significant challenges, resulting from its complex nature,[7] intrinsic heterogeneity deriving both from polymer biogenesis and extraction methodology,[8] and the still defective comprehension of its reactivity. To overcome these limitations, an emerging trend involves the production of lignin-based nanomaterials. While the existence of nanolignin was already known by micrographic studies of *Rezanowich* and *Goring* on lignosulfonates since the Sixties,[9] the beneficial effects of nanosizing lignin for obtaining high-value materials were not considered up to 2012, when Frangville et al. first described the production of lignin nanoparticles (LNPs).[10] Currently, robust literature is available on this class of nanomaterials, whose technological properties deriving from antibacterial, antioxidant, UV-absorbing, controlled-release, and adsorption capacity are currently being investigated in a plethora of applications, especially as substitutes of oil-based products.[11−21]

The production of LNPs, traditionally categorized into precipitation and nonprecipitation methods, has emerged as a transformative strategy to valorize industrial lignin.[22] Precipitation techniques, relying on solvent systems like THF, DMSO, or aqueous ethanol/acetone mixtures, are widely adopted for their simplicity but are often criticized for the environmental impact of nonrecoverable organic solvents.[10,14,23,24] To address these sustainability concerns,

Received: January 5, 2026
Revised: April 7, 2026
Accepted: April 9, 2026
Published: April 17, 2026

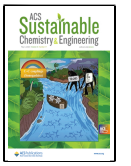

hydrotropic solutions (e.g., sodium *p*-tosylate) have been proposed as green, fully recoverable alternatives that facilitate higher lignin solubility and enhanced LNP yields.[25−29] Conversely, nonprecipitation methods utilizing physical (sonication/homogenization) or chemical (cross-linking with agents like epichlorohydrin) forces often suffer from limited morphological control and the potential toxicity of reticulating agents.[30,31] Recently, deep eutectic solvents and controlled self-assembly via π-π stacking have opened new avenues for producing ultrasmall, surfactant-free LNPs with superior stability.[32,33]

Beyond synthesis, recent research has shifted from basic structural assembly toward the development of high-value functional materials. A breakthrough study demonstrated the high-yield production of photonic glasses from LNPs,[34] where precise size control allows for tunable color across the visible spectrum, while, in the biomedical sector, LNPs were employed as delivery systems and showed good cellular internalization.[35,36]

The technical performance of LNPs is mainly influenced by two key characteristics: size and hydrophobicity. LNP size directly dictates biocompatibility and UV−vis absorption properties, with larger diameters often exhibiting superior biocompatibility.[37] Simultaneously, hydrophobicity determines the compatibility of LNPs within polymer matrices and influences the loading/release kinetics of active molecules.[38,39]

While traditional hydrophobization involves chemical modifications like etherification, esterification, or alkylation, these processes often rely on harsh reagents.[40,41] Catalytic oxidation, specifically utilizing laccases, represents a more sustainable alternative. Multicopper oxidases, such as laccases, operate under mild conditions using molecular oxygen as the sole electron acceptor, allowing for the concurrent tailoring of molecular weight and functional group density.[42−44]

Despite these advancements, a gap remains in integrating sequential fractionation with enzymatic modification to achieve control over the LNPs' properties. This study addresses this limitation by devising an easy and scalable multistep protocol for the tandem fractionation and laccase-mediated oxidation of hardwood kraft lignin (HKL). The approach illustrated here utilizes a transgenic laccase stable at alkaline pH, ensuring a homogeneous reaction environment for HKL and its acetone-insoluble (AIHKL) and acetone-soluble (ASHKL) fractions. This enables the production of enzymatically oxidized derivatives (HKLox, AIHKLox, and ASHKLox) with modulated molecular weights and hydrophobicity. By comparing LNPs generated via traditional ethanol:water precipitation against those formed in green sodium tosylate hydrotropes, this work establishes comprehensive structure−property relationships between enzymatic pretreatment and the resulting nanoparticle size and ζ-potential.

EXPERIMENTAL SECTION

Materials

The laccase used for this research was produced and kindly supplied by *Metgen* (Kaarina, Finand). Hardwood kraft lignin (HKL) was kindly supplied by *Westvaco* (Florence, South Carolina, USA). Reagent-grade acetone (Merck) was distilled and stored on activated 3A sieves before use. HPLC-grade dimethyl sulfoxide and deuterated chloroform were supplied by Macron Solvents and Cambridge Isotopes, respectively. All other reagents used, if not otherwise specified, were purchased in analytical-grade purity from Merck.

Lignin Fractionation

The isolation of AIHKL and ASHKL was performed according to the initial step of the extensive fractionation protocol reported by *Cui et al.*[45] Specifically, a 100 mg/mL dispersion of HKL in distilled acetone was stirred at room temperature for 12 h. Afterward, AIHKL was isolated from the mixture by vacuum filtration on a Büchner funnel. The precipitate was repeatedly washed with distilled acetone up to the disappearance of any residual traces of lignin from the filtrate (checked by TLC analysis *using Merck* alumina TLC plates with a UV-indicator, eluted using an acetone:NaOH 0.1 M, 9:1 mixture). The precipitate was then dried under vacuum at 40 °C overnight. ASHKL was obtained by rotary evaporation of acetone under vacuum at 40 °C.

Enzymatic Treatment

Enzymatic incubation of lignin was performed as previously described by Pajer et al. with slight implementations.[42] Specifically, lignin samples (2 mg/mL) were dissolved in an oxygen-saturated, pH 10.6 sodium glycinate buffer. The solution was transferred to a 40 °C thermostatic reactor equipped with a mechanical overhead stirrer and an inlet for bubbling air into the solution. The enzyme loading was determined based on: (i) the content of phenolic hydroxyl groups in the lignin sample, (ii) the amount of treated sample, (iii) the activity of the enzyme (determined via the ABTS test), and (iv) the reaction time. Specifically, one-hundred-fold excess of laccase with respect to the hydroxyl groups and an incubation time of 16 h under stirring (100 rpm) were selected to favor the complete oxidation of the treated substrates.[46] Subsequently, the solution was acidified to pH 1.5 with concentrated HCl to induce precipitation of the modified lignin. After 2 h, the precipitate was isolated by centrifugation (10 min, 4700 *g*) and washed with deionized water up to neutrality. The resulting oxidized lignin powder was lyophilized overnight and vacuum-dried at 40 °C for 24 h.

Spectrophotometric Determination of Laccase Activity via ABTS

The activity of the laccase solution was determined as follows: 900 μL of pH 4 buffer solution (50 mM, glycine hydrochloride) was mixed in a 2 mL quartz cuvette with 100 μL of a 20 mM Na_2ABTS [2,2′-azino-bis (3-ethylbenzthiazoline-6-sulfonic acid)disodium salt, spectroscopic grade] solution in ultrapure water. Afterward, 10 μL of a diluted laccase solution was added, the solution was vigorously mixed, and the absorbance variation of the solution was measured over 1 min at 420 nm using a Shimadzu UV−vis spectrophotometer.

The enzymatic activity (U/mL) of the laccase solution was determined using the following formula, taking into account the dilution factor:

$$\text{Enzyme activity} = \frac{\text{Absorbance variation } (\text{min}^{-1}) \times 1000\ \mu\text{L}}{21.2\frac{\text{mL}}{\mu\,\text{mol}\cdot\text{cm}} \times 10\ \mu\text{L} \times 1\ \text{cm}} \quad (1)$$

GPC Analysis

GPC analyses were performed on a Shimadzu HPLC system equipped with a UV−vis detector and a PLgel 5 μm MiniMIX-C column (Agilent). Specifically, lignin samples were dissolved in HPLC-grade DMSO, while HPLC-grade DMSO containing 0.1% lithium chloride was used as the eluent (solvent flow: 0.2 mL/min, elution temperature 70 °C). Standards of sulfonated polystyrene (4.3−2600 kDa) and lignin model compounds (170−941 Da) were used for the preparation of the calibration curve.

^{31}P NMR Analysis

The quantitative analyses of the hydroxyl groups in lignin samples was performed after derivatization with 2-chloro-4,4,5,5-tetramethyl-1,3-2-dioxaphospholane (TMDP, 98% Sigma-Aldrich) via ^{31}P NMR according to the methodology described by Argyropoulos et al.[47] Briefly, a precisely weighed amount of dry sample (overnight vacuum drying at 40 °C) was dissolved in a pyridine/deuterated chloroform mixture (1.6:1, v/v) in the presence of an internal standard

https://doi.org/10.1021/acssuschemeng.6c00142
ACS Sustainable Chem. Eng. 2026, 14, 8233−8243

(cholesterol) and chromium(III) acetylacetonate as a relaxation agent. The resulting solution was then derivatized using TMDP, and the spectrum was recorded on a 400 MHz Avance Bruker NMR spectrometer (128 scans, relaxation delay 12 s, acquisition delay 10 s).

Synthesis of LNPs

LNPs were prepared according to the solvent precipitation methods reported in Cailotto et al., with small modifications.[29] Specifically, for the hydrotropic protocol, 0.21 g of lignin was dispersed in 10 mL of 2 M sodium tosylate, while in the second protocol, 0.21 g of lignin was dispersed in 10 mL of a 70:30 ethanol:water (*v*/*v*) mixture. Both dispersions were stirred overnight and, afterward, subjected to centrifugation (15 min, 8422 *g*). Finally, the supernatant was filtered through a 0.24 μm PTFE syringe membrane. The filtrate, a clear solution, was dispersed dropwise into 30 mL of vigorously stirred (300 rpm) deionized water. The LNP dispersion was centrifuged as described above, and the supernatant was discarded. The precipitate was washed with deionized water until the sodium tosylate band disappeared in the UV−vis spectrum of the supernatant or three times in the case of the ethanol:water precipitation method. The resulting LNPs were finally dispersed in 100 mL of deionized water prior to further characterization.

To evaluate the yield of LNPs after their precipitation from the hydrotropic solution and the washing operations to remove the residual traces of sodium tosylate, the LNPs were dispersed in a volumetric flask. A 10 mL aliquot of the resulting dispersion was sampled and freeze-dried for yield determination.

Dynamic Light Scattering and ζ-Potential Analysis

The hydrodynamic diameter and size distribution of the LNPs were determined via dynamic light scattering (DLS) at pH 7.0. Measurements were performed using a Zetasizer Nano instrument (ZEN0040, Malvern Panalytical) at a 173° backscatter angle. LNP dispersions were diluted with deionized water to obtain a final concentration of 0.1 mg/mL, and the resulting mixtures were analyzed using a 1 mL spectroscopic-grade polyethylene cuvette (optical path 5 mm). The analyses were performed after 120 s of sample thermostated at 25 °C. The dispersing medium for the nanoparticles and the LNP refractive index were set, respectively, as "distilled water" and 1.511. Three sets of 13 scans each were performed per sample, and for each set, an average value was automatically calculated by the instrument. From these data, the average value of the three data sets was calculated and is reported here. In no case were multimodal LNP distributions obtained; consequently, an average value of the three sets was calculated, yielding the diameter for the nanoparticles as well as the polydispersity index. LNP colloidal stability was estimated via ζ-potential determination under the same conditions adopted for size analysis. The LNP colloidal dispersion was loaded into a disposable folded capillary cell (DTS1070, Malvern Panalytical) equipped with gold-plated beryllium−copper electrodes. The measurement voltage was automatically optimized by the instrument to ensure an ideal signal-to-noise ratio.

Scanning Electron Microscopy (SEM)

A field emission (FE) SEM Σigma VP (Zeiss) equipped with a thermal field emission gun (Schottky emitter) source was used to record images of the LNPs. Samples were deposited on a clean silicon wafer and analyzed at an acceleration voltage of 3 kV.

X-ray Photoelectron Spectroscopy (XPS)

The investigation of the surface chemistry of LNPs was performed using XPS analysis in Ultra High Vacuum (UHV, < 10^{-9} mBar) with a SPECS PHOIBOS 150 XPS system equipped with a monochromatic Al Kα (1486.6 eV) X-ray source. The samples were placed into a custom-made gold-coated copper sample holder. Considering the nature of the material, a full survey and O 1s core levels were investigated for each sample. The passing energy was set to 10 eV. Data fitting was performed using Kalibri KolXPD software and was based on previous literature on carbonaceous materials.[19,48−52]

From the C 1s, it is possible to deconvolute the spectra with peaks, each associated with a specific C moiety: the carbon sp^2 around 284.5 eV, the C sp^3 between 285 and 286 eV, and three main contributions of specific interest for the enzymatic oxidation of kraft lignin. Such contributions are alcohol/ethers (C−O/C−O−C) between 286 and 287 eV, aldehyde/ketones (O−C−O/C═O) in the range 287−288.5 eV, and esters/carboxyl groups (O−C═O/O═C−OH) between 288.5 and 290 eV.

RESULTS AND DISCUSSION

Isolation of HKL Fractions and Enzymatic Modification

HKL was fractionated into acetone-insoluble (AIHKL) and acetone-soluble (ASHKL) fractions, which were characterized via GPC and ^{31}P NMR. The chromatograms are summarized in Figure 1.

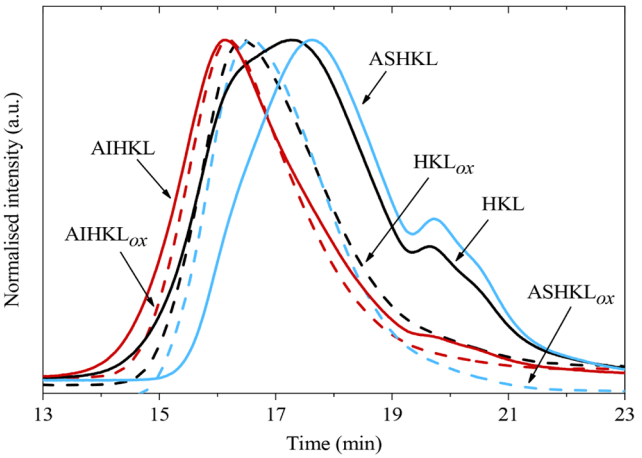

Figure 1. GPCs of the pristine lignin samples and their oxidized lignin ($_{ox}$) counterparts. HKL: hardwood kraft lignin, AIHKL: acetone-insoluble fraction, ASHKL: acetone-soluble fraction.

HKL is composed of 70.6% ASHKL, which shows a lower M_n than both HKL and the insoluble fraction. As expected, ASHKL contains a higher amount of phenolic groups than AIHKL and HKL, whereas AIHKL exhibits the highest content of aliphatic hydroxyl groups among the three lignin samples.[53] Notably, carboxylic acids are particularly abundant in ASHKL. This fact can be attributed to the presence of aliphatic (e.g., cinnamic acids) and aromatic carboxylic groups (e.g., benzoic acids), as well as muconic acids, the latter assumed to derive from the oxidation of lignin during the oxygen bleaching of kraft pulping.[54,55]

Subsequently, the oxidation treatment was carried out using a bacterial laccase capable of oxidizing lignin under alkaline conditions, thus ensuring a homogeneous reaction environment. Blanks were run under the same experimental conditions to account for the potential dissolution of a low molecular weight lignin soluble fraction. The number-average molecular weight (M_n), dispersity (Đ), and content of the various hydroxylated moieties for the oxidized lignin samples (HKL$_{ox}$, AIHKL$_{ox}$, and ASHKL$_{ox}$) are reported in Table 1, along with the data from the blank samples (HKL$_b$, AIHKL$_b$, and ASHKL$_b$).

The GPC analyses revealed the polymerizing effect of laccase, which resulted in a significant increase in the molecular weight for HKL and ASHKL. This increase was associated with a reduction in dispersity, a trend particularly evident in HKL. Conversely, laccase showed a reduced polymerizing effect on AIHKL, as AIHKL$_{ox}$ displayed only a slight increase in

https://doi.org/10.1021/acssuschemeng.6c00142
ACS Sustainable Chem. Eng. 2026, 14, 8233−8243

Table 1. Number Average Molecular Weight (M_n) and Dispersity (Đ) as Determined from GPC Analysis, and Functional Groups Occurrence (^{31}P NMR Analysis; Spectra Available in SI, Figure S1) for HKL, AIHKL, ASHKL, and the Corresponding Oxidised Samples (HKL_{ox}, $AIHKL_{ox}$, $ASHKL_{ox}$)

		Phenolic OH(mmol/g)[a]					
Sample	Aliphatic OH(mmol/g)[a]	Condensed/Syringyl	Noncondensed	Total	COOH[a] (mmol/g)	M_n	
HKL	1.36	0.50	1.98	2.48	1.66	1300	5.2
HKL_b	1.18	0.21	0.77	1.04	1.35	2000	4.3
HKL_{ox}	0.93	0	0.50	0.50	0.56	2700	3.6
ASHKL	1.03	0.38	1.91	2.29	1.65	950	3.8
$ASHKL_b$	0.85	0.29	0.87	1.16	1.20	1500	2.4
$ASHKL_{ox}$	0.72	0.19	0.47	0.66	0.89	2800	2.8
AIHKL	1.26	0.28	1.41	1.69	1.11	3900	3.3
$AIHKL_b$	1.07	0.14	0.58	0.72	0.95	4100	3.8
$AIHKL_{ox}$	0.91	0.24	0.56	0.80	0.80	4400	3.7

[a]Standard deviation for ^{31}P NMR analysis was calculated as 0.02 mmol/g.

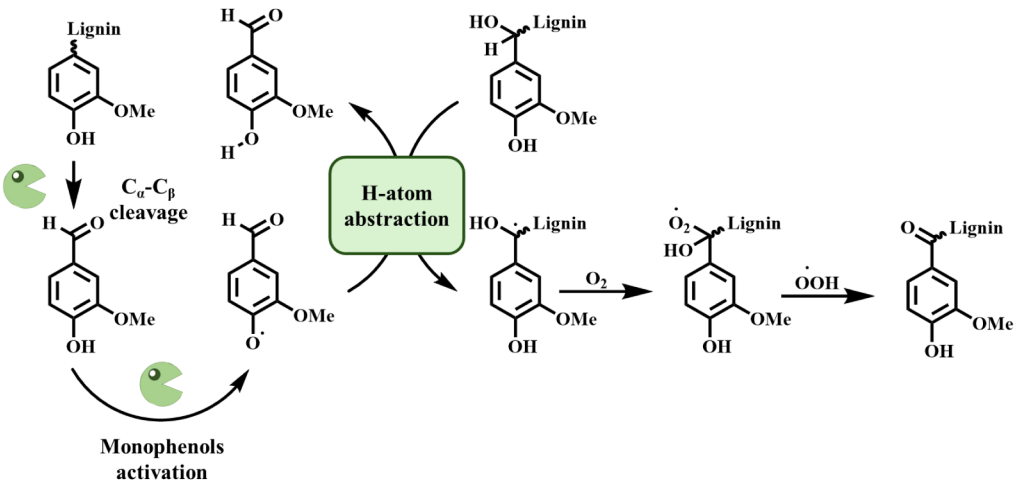

Figure 2. Proposed mechanism for the laccase-catalyzed oxidation of lignin aliphatic hydroxyl groups via redox mediators.

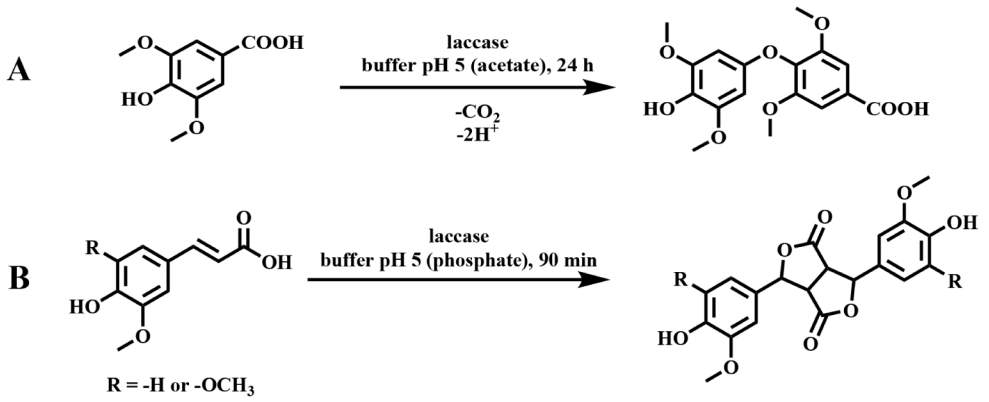

Figure 3. Laccase-catalyzed oxidation of carboxylic groups according to the two proposed mechanisms: A) formation of 4-O-1′ linkages[61] and B) *β-β′* coupling resulting in the formation of a pinoresinolide-like structure.[62]

molecular weight compared to both the starting and blank samples. This outcome can be attributed to the lower content of phenolic hydroxyl groups in AIHKL, resulting in a reduced number of sites for polymerization.

Furthermore, the peak shoulders appearing in the chromatograms of both HKL and ASHKL disappeared in the chromatograms of their oxidized counterparts (Figure 1). This testifies the concurrent occurrence of both a polymerization and a depolymerization process, the latter yielding water-soluble low molecular weight fractions that do not precipitate, in full agreement with previous reports.[42,44] ^{31}P NMR analyses further confirmed the efficacy of the laccase treatment, demonstrating that the overall content of all the different hydroxylated moieties decreased upon enzymatic oxidation (Table 1), leading to an enhancement of the hydrophobic character of the lignin molecules. Although an increase in the content of phenolic condensed units was not detected, the disappearance of phenolic hydroxyl groups was attributed to recondensation processes leading to the formation of new internal 4-O-5′ and 5,5′ units (*vide infra*).

https://doi.org/10.1021/acssuschemeng.6c00142
ACS Sustainable Chem. Eng. 2026, 14, 8233−8243

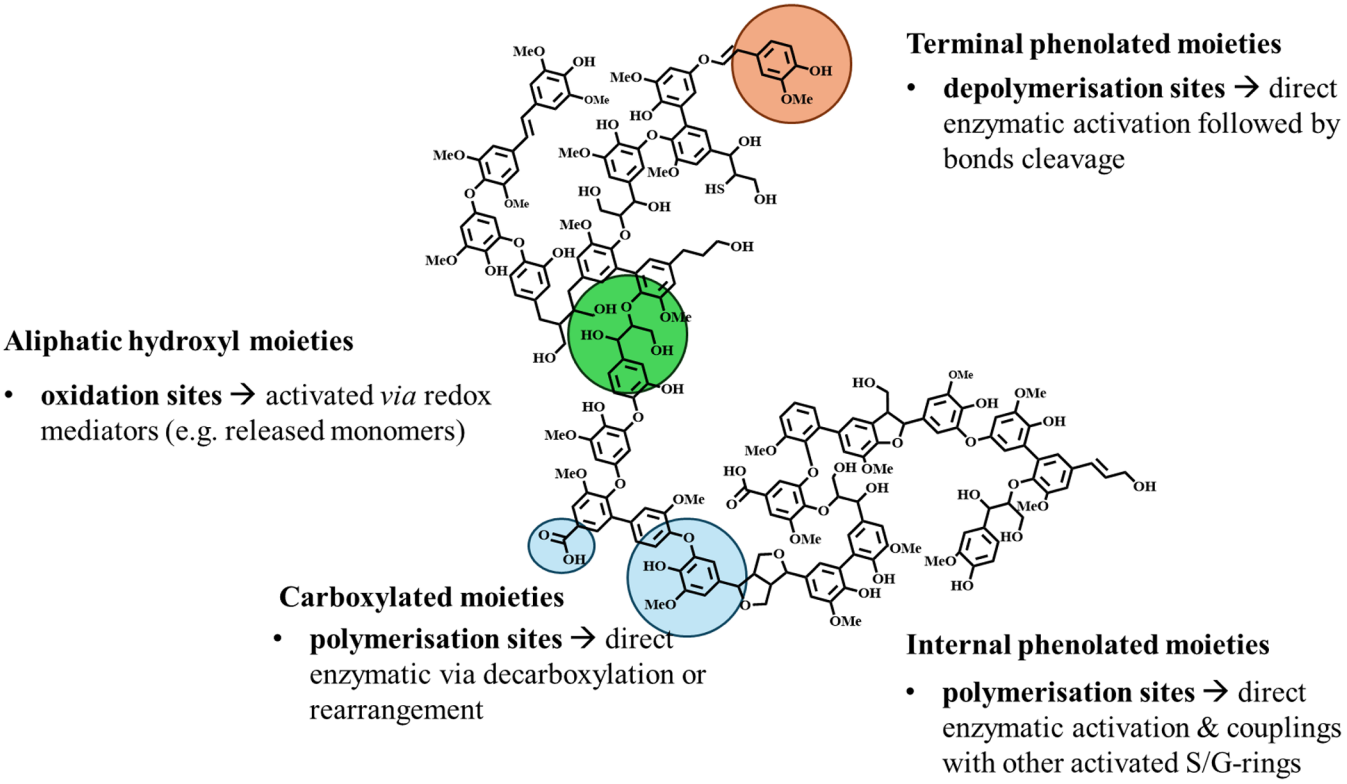

Figure 4. AIHKL substrates being converted during laccase-catalyzed oxidation.

This observation aligns with previous results,[42,46,56] suggesting the formation of endo-condensation sites, which cannot be revealed via lignin phosphitylation. The hypothesis is also supported by the observed increase in the molecular weight of the oxidized samples.

The decrease in the content of aliphatic hydroxyl groups can be explained considering the *in situ* generation of redox mediators deriving from the laccase-catalyzed depolymerization of lignin.[42,57−59] Specifically, once low molecular weight phenols (e.g., vanillin, syringin, acetovanillone, or acetosyringone) are formed upon the enzymatic degradation of the lignin via $C_\alpha C_\beta$-cleavage processes,[60] these compounds are quickly converted by the enzyme into aryloxy radicals. The latter easily diffuse onto lignin and subsequently act on benzylic carbons bearing a free hydroxyl group. In particular, benzylic radicals are formed via H atom abstraction, generating a substrate that can add O_2. The oxygen adduct then rearranges via the elimination of a hydroperoxide species, resulting in the formation of the C_α oxidation product, an acyl phenone. The proposed mechanism is rationalized in Figure 2.

This type of transformation is limited to benzylic hydroxyl groups, while primary hydroxyl groups do not undergo conversion into aldehydic groups. Interestingly, a significant decrease in the concentration of carboxylic acids was also observed in all of the treated samples. To rationalize this finding, two different reaction pathways can be considered based on the nature of the carboxylic groups involved. In the case of aromatic acids, the condensation of two units yielding the formation of a new 4-O-1' pattern with simultaneous decarboxylation (Figure 3A), as previously reported by Ikeda et al.,[61] could be hypothesized.

Conversely, in the case of aliphatic carboxylic acids, the *β-β'* coupling occurring on lignin motifs bearing the carboxylic group on C_γ is supposed to play a relevant role. As a matter of fact, ferulic and synapic acid may couple upon laccase treatment, resulting in the formation of pinoresinolide-like moieties where both C_γ form a lactone structure (Figure 3B) in accordance with early findings.[62]

The analyses of blanks demonstrated a decrease in hydroxyl group content, although to a much lower extent than the laccase-treated ones. This result was related to the presence of carbohydrate-based species, like glucuronic acids, which are formed in pulping conditions and remain trapped and absorbed on lignin during black liquor acidification. Reasonably, the neutralization of these acids caused by the sodium glycinate buffer would cause the formation of glucuronates, which are solubilized and removed during the washing steps.

The obtained data permit an overall rationalization of the behavior of hardwood kraft lignin upon laccase-catalyzed oxidation. AIHKL is generally considered structurally closer to native lignin, whereas ASHKL results from the recondensation of low molecular weight lignin fragments during the kraft cooking process.[53] For both fractions, the laccase-catalyzed modification involves similar general reaction pathways. In AIHKL, four types of substrates are involved (Figure 4): (a) terminal (orange, in Figure 4) and (b) internal (light blue, in Figure 4) phenolated moieties, (c) aliphatic hydroxyl groups (green, in Figure 4), and (d) carboxylic groups (light blue, in Figure 4). Besides the exodepolymerization on terminal units and the oxidation of Cα hydroxyl groups into ketones (Figure 2), polymerization also occurs. This effect is most likely uniquely attributed to the activation of internal phenolated moieties and their combination. Specifically, their conversion into aryloxy radicals is expected to proceed via activated guaiacyl units generating either (a) diaryl ethers (both

https://doi.org/10.1021/acssuschemeng.6c00142
ACS Sustainable Chem. Eng. 2026, 14, 8233−8243

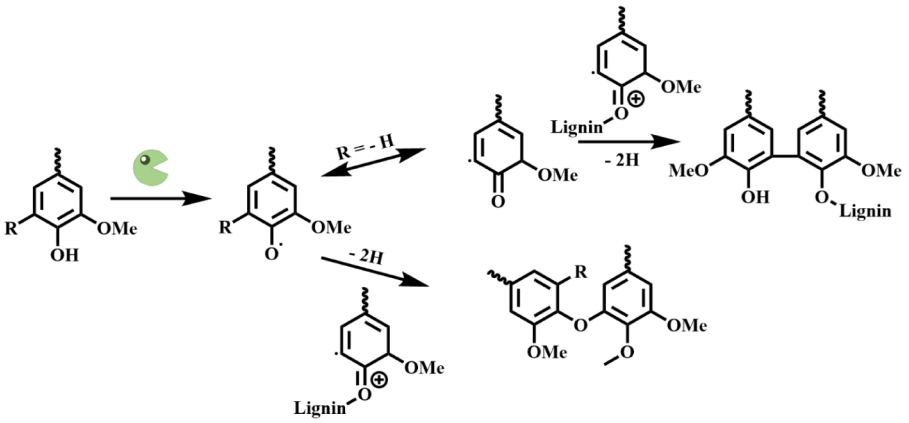

Figure 5. Laccase-catalyzed coupling of internal lignin aromatic nuclei via the generation of biphenyls (*up*) or diaryl ethers (*down*).

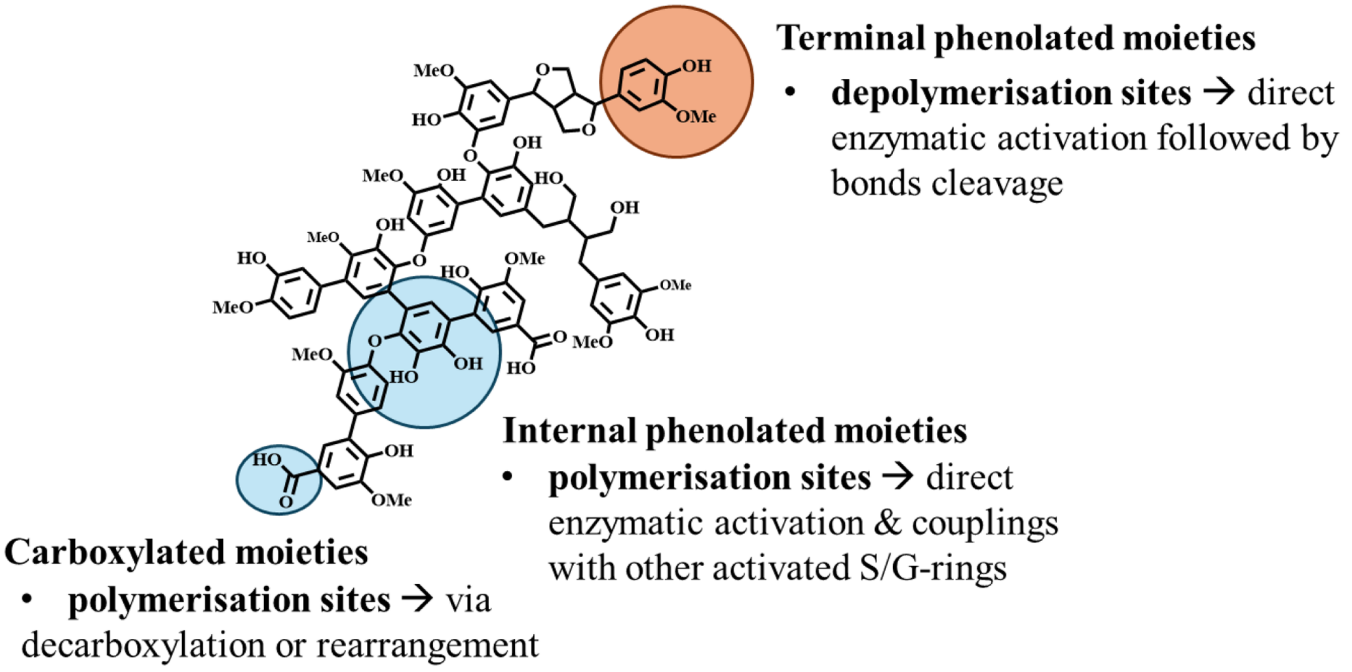

Figure 6. ASHKL units being converted during laccase-catalyzed oxidation.

Table 2. Yields, DLS, and ζ-Potential Data for LNPs from HKL, Its Fractions, and Their Enzymatically Modified Counterpart

Synthetic strategy	Source	LNPs	Yield (%)	Average diameter (nm)	PDI	ζ potential (mV)
Hydrotropic	HKL	**hHKL**	73.5	506 ± 24	0.475	−30 ± 1
	HKL_{ox}	**$hHKL_{ox}$**	76.8	740 ± 1	0.602	−32.7 ± 0.8
	AIHKL	**hAIHKL**	88.6	598 ± 25	0.220	−34 ± 2
	$AIHKL_{ox}$	**$hAIHKL_{ox}$**	97.1	766 ± 65	0.544	−42 ± 2
	ASHKL	**hASHKL**	63.2	492 ± 2	0.362	−30.7 ± 0.6
	$ASHKL_{ox}$	**$hASHKL_{ox}$**	59.4	617 ± 28	0.542	−30.8 ± 0.9
Ethanol:water mixture	HKL	**eHKL**	20.8	166 ± 3	0.422	−33.1 ± 0.5
	HKL_{ox}	**$eHKL_{ox}$**	56.7	175 ± 7	0.604	−33.3 ± 0.6
	AIHKL	**eAIHKL**	37.3	227 ± 5	0.596	−35.8 ± 0.9
	$AIHKL_{ox}$	**$eAIHKL_{ox}$**	66.6	220 ± 1	0.148	−40 ± 2
	ASHKL	**eASHKL**	11.7	176 ± 5	0.356	−32.1 ± 0.7
	$ASHKL_{ox}$	**$eASHKL_{ox}$**	63.8	192 ± 24	0.633	−31 ± 1

diguaiacyl or guaiacyl-syringyl ethers) via C_5-addition or (b) cross-coupling products leading to biphenyls (Figure 5).

ASHKL undergoes similar reaction pathways. Its major reactive sites are (Figure 6): (a) terminal (orange, in Figure 6) and (b) internal (light blue, in Figure 6) phenolated moieties and (c) carboxylic groups (light blue, in Figure 4). The terminal phenolics in ASHKL are expected to undergo the same exodepolymerization as in AIHKL forming new hydroxylated moieties either via C_α-C_β cleavages or via aryl-alkyl cleavages. These aliphatic hydroxyls can be subsequently

https://doi.org/10.1021/acssuschemeng.6c00142
ACS Sustainable Chem. Eng. 2026, 14, 8233−8243

oxidized by laccase possibly via redox-mediator-catalyzed oxidation, as depicted in Figure 2. On the other hand, internal phenolic groups and carboxylic groups are expected to react according to the mechanisms depicted in Figures 5 and 3, respectively.

Subsequently, HKL, ASHKL, AIHKL, and their enzymatically modified counterparts (HKL_{ox}, $ASHKL_{ox}$, and $AIHKL_{ox}$) were used for the preparation of LNPs.

LNPs Preparation and Characterization. The aggregation phenomena leading to the formation of LNPs were closely dependent on two main key parameters: (i) the structural differences of HKL, its fractions, and the corresponding laccase-treated samples and (ii) the synthetic strategies adopted. The combined action of these factors caused significant variations in the LNPs' yield, size, and surface properties. Nanosizing was achieved by means of two solvent precipitation protocols, i.e., lignin dissolution was facilitated by either a hydrotropic agent (sodium tosylate) or an ethanol:-water mixture, before the solution was diluted 10-fold in water, inducing lignin aggregation. The obtained LNPs, whose characterization data are reported in Table 2, are hereafter designated as hLNPs (via the hydrotropic method) and eLNPs (via the solvent-antisolvent method), respectively.

The ζ-potential was, as expected, negative in all cases, ranging from −30 mV to −42 mV. This range is indicative of good stability for the formed LNPs, effectively precluding aggregation phenomena.

The characterization data of the nanoparticles derived from HKL and its fractions reveal that HKL- and ASHKL-based LNPs exhibit similar size and yield. Conversely, AIHKL induced the formation of LNPs with larger diameters and higher yields compared with pristine HKL and its acetone-soluble fraction. This trend persists regardless of the synthetic strategy adopted, although the absolute values vary. This behavior can be explained by the relative composition of HKL. Indeed, while HKL is the sum of ASHKL and AIHKL, ASHKL accounts for over 70% of HKL's leaving AIHKL as the residual 30%. Consequently, HKL and ASHKL are structurally more alike, both in terms of hydroxyl group content and molecular weight, whereas AIHKL displays a much higher molecular weight and a reduced concentration of phenolic and carboxylic moieties (Figure 1 and Table 1). The higher yield can be attributed to the larger molecular weight of AIHKL which, upon dilution in water, facilitates the precipitation of a greater portion of the lignin molecules.

On the other hand, the increase in particle size is primarily determined by two main factors: (i) mechanism of LNPs growth and (ii) role of carboxylic groups. LNPs formation occurs through a layer-by-layer deposition process that begins with primary aggregates formed by the higher molecular weight lignin molecules followed by the deposition of lower molecular weight molecules.[38] Since a larger fraction of AIHKL precipitates due to its greater insolubility in the solvent systems compared to HKL and ASHKL, the latter deposit on the surface of the forming lignin particles, leading to the generation of larger LNPs. Additionally, the content of carboxyl groups, which is particularly significant in this kraft lignin, also plays a crucial role. Specifically, the lower the content of carboxylic groups, reduced of about 33% in AIHKL with respect to HKL and ASHKL, the larger the particle size.

Under the investigated aggregation conditions, the low pK_a ($\approx$ 4.2) of the carboxylic groups ensures they exist predominantly as carboxylates. It is hypothesized that this negative charge limits particle size through two primary mechanisms: first, electrostatic stabilization increases inter-particle repulsion, thereby inhibiting aggregation; second, the carboxylates engage in strong interactions with neighboring hydroxyl groups, resulting in more compact particle architectures. As the content of carboxylates is reduced (as in AIHKL), these interactions are lessened, driving the formation of a less compact particle structure and thus larger LNPs.

The result here reported on the size of the LNPs synthesized by the hydrotropic method differs significantly from previously published data. Specifically, in a recent study[63] the dimensions of LNPs derived from HKL and its acetone-soluble and acetone-insoluble fractions were approximately 300 nm, 450 nm, and 150 nm, respectively. While the yields in the above-mentioned work are comparable to those presented here, the differences in terms of dimensions are significant. Not only does the absolute size of the LNPs vary but also the trend among the three samples is different from our findings. A comparison of the molecular characterization data reveals that the lignins used in both studies possess comparable molecular weight but show a considerable variation in the content of phenolics and carboxylic acids, respectively reduced by about 30−40% and increased by 3.5 times compared to the work of Colucci et al. Although these differences should not be neglected, more importantly, the LNPs' preparation protocol differs in a key factor, as in this work, the lignin solution was added dropwise to water, while in Colucci et al., water was rapidly added to the lignin solution. Therefore, these findings confirm that the way the lignin molecules are induced to aggregate plays a crucial role in the self-assembly process, significantly affecting the final size for the formed LNPs, and underscores the importance of standardized synthesis protocols for a reliable and direct comparison of LNPs' properties.[64]

The properties of the LNPs synthesized here can be further understood by comparing samples derived from laccase-oxidized lignins to those from untreated lignins. Using the hydrotropic strategy, the size of the generated LNPs increases in all cases when oxidized lignins are used, while the yields remain practically unchanged. This suggests that the enzymatic treatment does not significantly improve the lignin solubility within the hydrotropic system. Therefore, the observed size increase can be attributed to a reduction in the packing density of the LNPs compared to those derived from unoxidized lignin. This decreased density likely arises from two main factors: (i) the increased molecular weight resulting from laccase treatment restricts efficient chain folding during LNP assembly, and (ii) the depletion of hydroxyl and carboxylic groups upon oxidation diminishes the availability of hydrogen-bonding sites. In contrast, when employing the ethanol:water precipitation protocol, LNPs derived from oxidized lignins exhibit sizes comparable to those synthesized from untreated counterparts, despite a marked increase in yield. In this case, it can be hypothesized that the laccase-mediated reduction of hydroxyl and carboxylic groups improves the lignin solubility within this specific solvent system, in turn facilitating the nucleation of a greater number of LNPs. Furthermore, SEM analysis on LNPs derived from both pristine and oxidized HKL confirms that a consistently globular, spherical morphology is maintained regardless of the oxidation treatment (Figure S2).

Finally, the findings of this work can be discussed by directly comparing the LNPs obtained from two distinct synthetic approaches. In a general observation, the LNPs produced using

https://doi.org/10.1021/acssuschemeng.6c00142
ACS Sustainable Chem. Eng. 2026, 14, 8233−8243

ethanol:water mixtures are smaller than their corresponding counterparts generated via the hydrotropic method. However, a mechanistic explanation is not straightforward because the yield also changes significantly between the methods and, as previously described, many factors contribute to this outcome.

Nevertheless, a key comparison can be made between hASHKL$_{ox}$ and eASHKL$_{ox}$, which display very similar yields but considerably different particle sizes, with hASHKL$_{ox}$ being approximately three times larger. In this case, lignin solubility in the solvent system as a key difference can be excluded given that the final LNP yields are comparable. Additionally, since both LNPs originated from the same lignin sample (ASHKL$_{ox}$), differences in the starting lignin's structural characteristics as a factor can be eliminated. On these bases, the obtained results can be rather explained by considering the different solvation mechanisms for lignin in the hydrotrope versus the ethanol: water mixture.

Specifically, the physical phenomenon underpinning lignin dissolution in hydrotropic solutions relies on the formation of π-π' interactions between the aromatic rings of the neutralized tosylate anions and the aromatic rings on lignin. The tosylate anions effectively penetrate the lignin structure, causing its unfolding by intercalating between the interacting aromatic domains of the lignin molecules, thereby disrupting the π-π' stacking. Consequently, lignin undertakes a more elongated structure, occupying a larger hydrodynamic volume than in the ethanol:water mixture. Indeed, lignin dissolution in the ethanol:water mixture is due to the formation of hydrogen bonds with the solvent molecules, which replace the existing intramolecular hydrogen bonds within the lignin structure, while the π-π stacking interactions between the lignin rings are most likely unaltered. This, combined with the presence of nonpolar ethyl chains, is suggested to induce a hydrophobic collapse of the lignin structure, resulting in a globular conformation, as previously described.[65]

Subsequently, during the dilution step leading to LNP formation, interactions between the lignin molecules and water rapidly occur. Since water-lignin interactions have been demonstrated to have much faster kinetics than lignin conformational rearrangements,[65] this difference in the initial lignin structure is preserved.

In the hydrotropic mixture, the π-π' stacking interactions cleaved during dissolution cannot be reestablished, and the lignin molecules retain their elongated structure. This arrangement gives rise to less compact and therefore larger LNPs. Conversely, the globular structure assumed during dissolution in the ethanol:water mixture allows for the formation of more packed and denser LNPs, resulting in a smaller size. This occurs because during the formation of LNPs, the hydrogen bonds between lignin and the solvent are replaced with new lignin−lignin interactions without disrupting the fundamentally compact globular structure.

The impact of fractionation and biocatalytic oxidation on the surface chemistry of hLNPs was investigated via XPS analysis, as this technique probes only the outermost few nanometers of the LNPs, thereby allowing for a specific evaluation of their surface interface. Each sample was analyzed based on carbon moieties derived from the deconvolution of the C 1s core levels (data not shown). The resulting chemical speciation is presented in Figure 7, summarizing the deconvolution and moiety fractions identified.

Averaged binding energies (BE) across samples revealed consistent peak positioning: defective carbon (Def. C) at 283.7 ± 0.2 eV, the Csp^2 component at 284.7 ± 0.2 eV, C−C and C−H species (assigned to Csp^3) at 285.5 ± 0.1 eV, and three primary oxygenated peaks at 286.4 ± 0.2 eV (C−O/C−O−C), 287.3 ± 0.2 eV (C═O), and 289.0 ± 0.1 eV (O−C═O/O═C−OH). Comparing the relative surface carbon content of LNPs derived from pristine lignin and its two fractions prior to enzymatic oxidation reveals that the variation in functional groups, previously identified in the bulk by ^{31}P NMR, is preserved on the nanoparticles' surface. Specifically, hHKL and hASHKL exhibit higher sp^2 and lower sp^3 carbon contents compared to hAIHKL, reflecting the reduced phenolic character of the latter. Furthermore, hHKL and hASHKL expose a greater density of hydroxyl and ether groups than hAIHKL. This surface similarity between hHKL and hASHKL is consistent with the core−shell formation mechanism of LNPs from HKL, where the acetone-soluble fraction constitutes the shell and the insoluble fraction forms the core of the particles. Subsequent laccase treatment did not significantly alter the overall surface sp^2/sp^3 ratio of each sample, yet it induced a marked reduction in hydroxyl groups and a concomitant increase in ketone moieties across hHKL$_{ox}$, hAIHKL$_{ox}$, and hASHKL$_{ox}$.

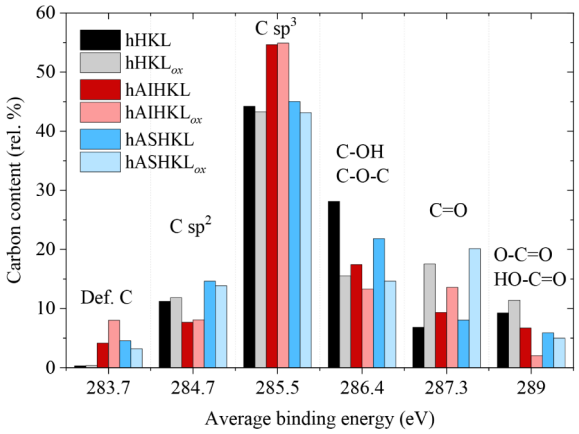

Figure 7. Summary of the C 1s deconvolution highlighting the functional groups present on the surface of the LNPs. The binding energies plotted are meant as average values among the samples, as reported in the main text. Def. C: defective carbon. (XPS diffractograms are reported in SI, Figures S3, S4, and S5).

Quantitatively, enzymatic oxidation reduced C−OH functionalities by 45%, 24%, and 33%, and increased C═O groups by 2.6, 1.5, and 2.5 times for LNPs derived from HKL, AIHKL, and ASHKL, respectively. This demonstrates effective surface hydrophobization, a result that is particularly significant considering that LNP formation via aqueous precipitation typically drives polar groups to the surface. Similarly to the fractionation step, hHKL$_{ox}$ and hASHKL$_{ox}$ responded comparably to oxidation, whereas hAIHKL$_{ox}$ exhibited less pronounced variations. This behavior correlates well with the molecular structure of the fractions. Although the oxidative treatment reduced the overall concentration of hydroxyl groups, the significant aliphatic chain content in AIHKL afforded greater chain mobility. This facilitates the reorientation and exposure of residual hydroxyls at the nanoparticle surface, thereby resulting in a smaller observed reduction in surface hydroxyl content compared to that of ASHKL.

https://doi.org/10.1021/acssuschemeng.6c00142
ACS Sustainable Chem. Eng. 2026, 14, 8233−8243

CONCLUSIONS

This study establishes a novel and robust framework for the controlled engineering of LNPs by implementing a synergistic two-step pretreatment of hardwood kraft lignin. By integrating acetone-based fractionation with laccase-mediated oxidative modification, five distinct lignin preparations were isolated (AIHKL, ASHKL, and the oxidized counterparts), each exhibiting reduced dispersity and specific structural features.

A key finding of this work is the biocatalytic effect of laccase, which facilitated a significant increase in molecular weight, most notably a 3-fold enhancement in $ASHKL_{ox}$ fraction, while simultaneously modifying the lignins' functional groups, such as successfully lowering the concentration of carboxylic groups via the condensation of aromatic acids and the coupling of aliphatic carboxylic acids, which respectively yielded novel 4-O-1' and β-β' moieties.

Furthermore, this research provides a comprehensive mechanistic rationalization of LNP formation. The growth of LNPs, which follows a layer-by-layer deposition model where lower molecular weight molecules deposit onto primary aggregates of larger molecules, is governed by a complex interplay between: (i) functional group density, as the hydroxyl and carboxyl content dictate the extent of hydrogen bonding, determining the structural integrity of the LNPs; (ii) molecular weight, which influences chain folding kinetics and overall lignin solubility; and (iii) solvation mechanism, since the choice of solvent is identified as a critical determinant of size and structure. Indeed, the use of the hydrotropic sodium tosylate solution induced an unfolding of the lignin structure via π-π' interactions, which, upon rapid precipitation, yielded larger LNPs with diameters up to 750 nm. In contrast, the ethanol:water system promoted hydrophobic collapse of the lignin structure, producing denser, sub-230 nm particles. Finally, the oxidative treatment proved to be a powerful tool for surface chemistry modulation, increasing LNP hydrophobicity by reducing surface hydroxyls by up to 45% and enriching ketone functionalities by 1.5−2.6 times.

Collectively, these results provide clear insights into the rational design of LNPs, offering a versatile platform for the development of high-performance bionanocomposites and advanced sustained-release systems.

ASSOCIATED CONTENT

Supporting Information

The Supporting Information is available free of charge at https://pubs.acs.org/doi/10.1021/acssuschemeng.6c00142.

^{31}P NMR spectra and X-ray photoemission spectroscopy deconvoluted spectra of C 1s and O 1s core levels of pristine and enzymatically treated lignin samples; SEM micrographs of LNPs (PDF)

AUTHOR INFORMATION

Corresponding Author

Matteo Gigli − *Department of Molecular Sciences and Nanosystems, Ca' Foscari University of Venice, Venice 30172, Italy;* orcid.org/0000-0003-3899-0399; Email: matteo.gigli@unive.it

Authors

Nicolò Pajer − *Department of Molecular Sciences and Nanosystems, Ca' Foscari University of Venice, Venice 30172, Italy;* Present Address: Department of Bioproducts and Biosystems, School of Chemical Engineering, Aalto University, Vuorimiehentie 1, 02150 Espoo, Finland

Valerio C. A. Ficca − *TERIN Department, Division of Technologies and Vectors for Decarbonization, ENEA Casaccia Research Center, Rome 00123, Italy; Department of Physics, Sapienza University of Rome, Rome 00185, Italy*

Ernesto Placidi − *Department of Physics, Sapienza University of Rome, Rome 00185, Italy;* orcid.org/0000-0002-3820-8451

Dimitris S. Argyropoulos − *Department of Forest Biomaterials, North Carolina State University, Raleigh, North Carolina 27695, United States of America*

Claudia Crestini − *Department of Molecular Sciences and Nanosystems, Ca' Foscari University of Venice, Venice 30172, Italy;* orcid.org/0000-0001-9903-2675

Complete contact information is available at: https://pubs.acs.org/10.1021/acssuschemeng.6c00142

Notes

The authors declare no competing financial interest.

ACKNOWLEDGMENTS

NP, MG, and CC would like to express their gratitude to the B-LigZymes project (EU Rise H2020, number 824017) for funding part of this research, as well as Metgen (Kaarina, Finland) for supplying the enzyme used in this research. The XPS experiments were carried out at the SmartLab departmental laboratory of the Department of Physics at Sapienza University of Rome.

REFERENCES

(1) Browning, B. L. The Composition and Chemical Reactions of Wood. *The Chemistry of Wood*; Interscience Publisher; New York, pp. 57−102.

(2) Bajwa, D. S.; Pourhashem, G.; Ullah, A. H.; Bajwa, S. G. A Concise Review of Current Lignin Production, Applications, Products and Their Environmental Impact. *Ind. Crops Prod.* **2019**, *139*, 111526.

(3) Väisänen, T.; Das, O.; Tomppo, L. A Review on New Bio-Based Constituents for Natural Fiber-Polymer Composites. *J. Clean. Prod.* **2017**, *149*, 582−596.

(4) Collard, F.-X.; Blin, J. A Review on Pyrolysis of Biomass Constituents: Mechanisms and Composition of the Products Obtained from the Conversion of Cellulose, Hemicelluloses and Lignin. *Renewable Sustainable Energy Rev.* **2014**, *38*, 594−608.

(5) Paananen, H.; Pakkanen, T. T. Kraft Lignin Reaction with Paraformaldehyde. *Holzforschung* **2020**, *74* (7), 663−672.

(6) Ragauskas, A. J.; Beckham, G. T.; Biddy, M. J.; Chandra, R.; Chen, F.; Davis, M. F.; Davison, B. H.; Dixon, R. A.; Gilna, P.; Keller, M.; et al. Lignin Valorization: Improving Lignin Processing in the Biorefinery. *Science* **2014**, *344* (6185), 1246843.

(7) Ragauskas, A. J.; Beckham, G. T.; Biddy, M. J.; Chandra, R.; Chen, F.; Davis, M. F.; Davison, B. H.; Dixon, R. A.; Gilna, P.; Keller, M.; et al. Present and Future. *Wood Sci. Technol.* **1977**, *11* (3), 169−218.

(8) Gigli, M.; Crestini, C. Fractionation of Industrial Lignins: Opportunities and Challenges. *Green Chem.* **2020**, *22* (15), 4722−4746.

(9) Rezanowich, A.; Yean, W. Q.; Goring, D. A. I. High Resolution Electron Microscopy of Sodium Lignin Sulfonate. *J. Appl. Polym. Sci.* **1964**, *8* (4), 1801−1812.

(10) Frangville, C.; Rutkevičius, M.; Richter, A. P.; Velev, O. D.; Stoyanov, S. D.; Paunov, V. N. Fabrication of Environmentally Biodegradable Lignin Nanoparticles. *ChemPhyschem* **2012**, *13* (18), 4235−4243.

(11) Yang, W.; Owczarek, J. S.; Fortunati, E.; Kozanecki, M.; Mazzaglia, A.; Balestra, G. M.; Kenny, J. M.; Torre, L.; Puglia, D. Antioxidant and Antibacterial Lignin Nanoparticles in Polyvinyl Alcohol/Chitosan Films for Active Packaging. *Ind. Crops Prod.* **2016**, *94*, 800−811.
(12) Yang, W.; Fortunati, E.; Bertoglio, F.; Owczarek, J. S.; Bruni, G.; Kozanecki, M.; Kenny, J. M.; Torre, L.; Visai, L.; Puglia, D. Polyvinyl Alcohol/Chitosan Hydrogels with Enhanced Antioxidant and Antibacterial Properties Induced by Lignin Nanoparticles. *Carbohydr. Polym.* **2018**, *181*, 275−284.
(13) Domenek, S.; Louaifi, A.; Guinault, A.; Baumberger, S. Potential of Lignins as Antioxidant Additive in Active Biodegradable Packaging Materials. *J. Polym. Environ.* **2013**, *21* (3), 692−701.
(14) Tian, D.; Hu, J.; Bao, J.; Chandra, R. P.; Saddler, J. N.; Lu, C. Lignin Valorization: Lignin Nanoparticles as High-Value Bio-Additive for Multifunctional Nanocomposites. *Biotechnol. Biofuels* **2017**, *10* (1), 192.
(15) Figueiredo, P.; Ferro, C.; Kemell, M.; Liu, Z.; Kiriazis, A.; Lintinen, K.; Florindo, H. F.; Yli-Kauhaluoma, J.; Hirvonen, J.; Kostiainen, M. A.; Santos, H. A. Functionalization of Carboxylated Lignin Nanoparticles for Targeted and pH-Responsive Delivery of Anticancer Drugs. *Nanomedicine* **2017**, *12* (21), 2581−2596.
(16) Lievonen, M.; José Valle-Delgado, J.; Mattinen, M.-L.; Hult, E.-L.; Lintinen, K. A.; Kostiainen, M.; Paananen, A. R.; Szilvay, G.; Setälä, H.; Österberg, M. A Simple Process for Lignin Nanoparticle Preparation. *Green Chem.* **2016**, *18* (5), 1416−1422.
(17) Sipponen, M. H.; Lange, H.; Crestini, C.; Henn, A.; Österberg, M. Lignin for Nano- and Microscaled Carrier Systems: Applications, Trends, and Challenges. *ChemSuschem* **2019**, *12* (10), 2039−2054.
(18) Xing, Q.; Buono, P.; Ruch, D.; Dubois, P.; Wu, L.; Wang, W.-J. Biodegradable UV-Blocking Films through Core−Shell Lignin−Melanin Nanoparticles in Poly(Butylene Adipate-Co-Terephthalate). *ACS Sustainable Chem. Eng.* **2019**, *7* (4), 4147−4157.
(19) Rahimihaghighi, M.; Gigli, M.; Ficca, V. C. A.; Placidi, E.; Sgarzi, M.; Crestini, C. Lignin-Derived Sustainable Nano-Platforms: A Multifunctional Solution for an Efficient Dye Removal. *ChemSuschem* **2024**, *17* (24), No. e202400841.
(20) Moreno, A.; Sipponen, M. H. Overcoming Challenges of Lignin Nanoparticles: Expanding Opportunities for Scalable and Multifunctional Nanomaterials. *Acc. Chem. Res.* **2024**, *57* (14), 1918−1930.
(21) Yang, W.; Ding, H.; Qi, G.; Guo, J.; Xu, F.; Li, C.; Puglia, D.; Kenny, J.; Ma, P. Enhancing the Radical Scavenging Activity and UV Resistance of Lignin Nanoparticles via Surface Mannich Amination toward a Biobased Antioxidant. *Biomacromolecules* **2021**, *22* (6), 2693−2701.
(22) Pajer, N.; Cestari, C.; Argyropoulos, D. S.; Crestini, C. From Lignin Self Assembly to Nanoparticles Nucleation and Growth: A Critical Perspective. *Npj Mater. Sustain.* **2024**, *2* (1), 1−9.
(23) Richter, A. P.; Bharti, B.; Armstrong, H. B.; Brown, J. S.; Plemmons, D.; Paunov, V. N.; Stoyanov, S. D.; Velev, O. D. Synthesis and Characterization of Biodegradable Lignin Nanoparticles with Tunable Surface Properties. *Langmuir* **2016**, *32* (25), 6468−6477.
(24) Qian, Y.; Deng, Y.; Qiu, X.; Li, H.; Yang, D. Formation of Uniform Colloidal Spheres from Lignin, a Renewable Resource Recovered from Pulping Spent Liquor. *Green Chem.* **2014**, *16* (4), 2156−2163.
(25) Chen, L.; Dou, J.; Ma, Q.; Li, N.; Wu, R.; Bian, H.; Yelle, D. J.; Vuorinen, T.; Fu, S.; Pan, X.; et al. Rapid and Near-Complete Dissolution of Wood Lignin at ≤ 80°C by a Recyclable Acid Hydrotrope. *Sci. Adv.* **2017**, *3* (9), No. e1701735.
(26) Chen, L.; Zhou, X.; Shi, Y.; Gao, B.; Wu, J.; Kirk, T. B.; Xu, J.; Xue, W. Green Synthesis of Lignin Nanoparticle in Aqueous Hydrotropic Solution toward Broadening the Window for Its Processing and Application. *Chem. Eng. J.* **2018**, *346*, 217−225.
(27) Ma, Q.; Zhu, J.; Gleisner, R.; Yang, R.; Zhu, J. Y. Valorization of Wheat Straw Using a Recyclable Hydrotrope at Low Temperatures (≤90 °C). *ACS Sustainable Chem. Eng.* **2018**, *6* (11), 14480−14489.
(28) Yang, M.; Zhang, X.; Guan, S.; Dou, Y.; Gao, X.; Miao, L. Green Preparation of Lignin Nanoparticles in an Aqueous Hydrotropic Solution and Application in Biobased Nanocomposite Films. *Holzforschung* **2021**, *75* (5), 463−473.
(29) Cailotto, S.; Gigli, M.; Bonini, M.; Rigoni, F.; Crestini, C. Sustainable Strategies in the Synthesis of Lignin Nanoparticles for the Release of Active Compounds: A Comparison. *ChemSuschem* **2020**, *13* (17), 4759−4767.
(30) Nair, S. S.; Sharma, S.; Pu, Y.; Sun, Q.; Pan, S.; Zhu, J. Y.; Deng, Y.; Ragauskas, A. J. High Shear Homogenization of Lignin to Nanolignin and Thermal Stability of Nanolignin-Polyvinyl Alcohol Blends. *ChemSuschem* **2014**, *7* (12), 3513−3520.
(31) Nypelö, E. T. A.; Carrillo, C. J.; Rojas, O. Lignin Supracolloids Synthesized from (W/O) Microemulsions: Use in the Interfacial Stabilization of Pickering Systems and Organic Carriers for Silver Metal. *Soft Matter* **2015**, *11* (10), 2046−2054.
(32) Yue, X.; Lin, J.; Mankinen, O.; Suopajärvi, T.; Mikola, M.; Mikkelson, A.; Huttunen, H.; Chen, L.; Ahola, J.; Telkki, V.-V.; Sun, S.; Liimatainen, H. Lignin Dissolution and Direct Ultrasmall-Lignin-Nanoparticle Formation in Acidic and Alkaline Deep Eutectic Solvents: A Molecular-Level Insight. *Angew. Chem. Int. Ed.* **2025**, *64* (30), No. e202505975.
(33) Senra, L. F.; Fernandes Pereira, P. H.; Camani, P. H.; Arantes, V.; Rosa, D. S.; Mulinari, D. R. Lignin Nanoparticle-Reinforced Starch Aerogel: Eco-Designed Adsorbent for Water Remediation. *Bioresour. Technol.* **2026**, *445*, 134056.
(34) Thalakkale Veettil, U.; Huertas-Alonso, A. J.; Plivelic, T. S.; Sipponen, M. H. High-Yield Production of Lignin Nanoparticle Photonic Glasses. *Green Chem.* **2025**, *27* (7), 2130−2137.
(35) Mavali Zadeh, A.; Gatto, E.; Lettieri, R.; Bokharaie, H.; Caravella, A.; D'Ottavi, C.; Di Bartolomeo, E.; Domenici, F.; Sima, S.; Correia, A.; Rauniyar, K.; Klose, A.; Gounani, Z.; Laaksonen, T.; Künnapuu, J.; Jeltsch, M. Biomass-Derived Lignin Nanoparticles for the Sustained Delivery of Vascular Endothelial Growth Factor-C. *Eur. J. Pharm. Biopharm.* **2025**, *216*, 114860.
(36) Figueiredo, P.; Sipponen, M. H.; Lintinen, K.; Correia, A.; Kiriazis, A.; Yli-Kauhaluoma, J.; Österberg, M.; George, A.; Hirvonen, J.; Kostiainen, M. A.; Santos, H. A. Preparation and Characterization of Dentin Phosphophoryn-Derived Peptide-Functionalized Lignin Nanoparticles for Enhanced Cellular Uptake. *Small* **2019**, *15* (24), 1901427.
(37) Cestari, C.; Pajer, N.; Crestini, C. Aggregation Phenomena in Lignin. In *Reference Module in Chemistry, Molecular Sciences and Chemical Engineering*; Elsevier, 2024. DOI: .
(38) Zhou, M.; Xiong, Z.; Yang, D.; Pang, Y.; Wang, D.; Qiu, X. Preparation of Slow Release Nanopesticide Microspheres from Benzoyl Lignin. *Holzforschung* **2018**, *72* (7), 599−607.
(39) Li, B.; You, S.; Qi, W.; Wang, Y.; Su, R.; He, Z. Structure-Tunable Assembly of Lignin Sub-Micro Spheres by Modifying the Amphiphilic Interfaces of Lignin via n-Alkane. *Eur. Polym. J.* **2020**, *126*, 109539.
(40) Duval, A.; Avérous, L. Mild and Controlled Lignin Methylation with Trimethyl Phosphate: Towards a Precise Control of Lignin Functionality. *Green Chem.* **2020**, *22* (5), 1671−1680.
(41) Johansson, M.; Skrifvars, M.; Kadi, N.; Dhakal, H. N. Effect of Lignin Acetylation on the Mechanical Properties of Lignin-Poly-Lactic Acid Biocomposites for Advanced Applications. *Ind. Crops Prod.* **2023**, *202*, 117049.
(42) Pajer, N.; Gigli, M.; Crestini, C. The Laccase Catalysed Tandem Lignin Depolymerisation/Polymerisation. *ChemSuschem* **2024**, *17* (15), No. e202301646.
(43) Boarino, A.; Charmillot, J.; Figueirêdo, M. B.; Le, T. T. H.; Carrara, N.; Klok, H.-A. Ductile High-Lignin-Content Thermoset Films and Coatings. *ACS Sustainable Chem. Eng.* **2023**, *11* (46), 16442−16452.
(44) Vignali, E.; Gigli, M.; Cailotto, S.; Pollegioni, L.; Rosini, E.; Crestini, C. The Laccase-Lig Multienzymatic Multistep System in Lignin Valorization. *ChemSuschem* **2022**, *15* (20), No. e202201147.
(45) Cui, C.; Sun, R.; Argyropoulos, D. Fractional Precipitation of Softwood Kraft Lignin: Isolation of Narrow Fractions Common to a Variety of Lignins. *ACS Sustain. Chem. Eng.* **2014**, *2* (4), 959−968.

https://doi.org/10.1021/acssuschemeng.6c00142
ACS Sustainable Chem. Eng. 2026, 14, 8233−8243

(46) Pajer, N.; Gigli, M.; Crestini, C. The Laccase Catalysed Tandem Lignin Depolymerisation/Polymerisation. *ChemSusChem* **2024**, *17* (n/a), No. e202301646.
(47) Meng, X.; Crestini, C.; Ben, H.; Hao, N.; Pu, Y.; Ragauskas, A. J.; Argyropoulos, D. S. Determination of Hydroxyl Groups in Biorefinery Resources via Quantitative 31 P NMR Spectroscopy. *Nat. Protoc.* **2019**, *14* (9), 2627−2647.
(48) Sallaku, L.; Mirizzi, L.; Muhyuddin, M.; Ficca, V. C. A.; Placidi, E.; Lamanna, N.; Zoia, L.; Vassalini, I.; Federici, S.; Berretti, E.; Filippi, J.; Lavacchi, A.; Binetti, S.; Mustarelli, P.; Santoro, C. Upgrading the Waste Acrylonitrile-Butadiene-Styrene into Crude Oil and Highly Efficient Electrocatalysts for Oxygen Reduction Reaction. *Chem. Eng. J.* **2025**, *512*, 162236.
(49) Zuccante, G.; Muhyuddin, M.; Ficca, V. C. A.; Placidi, E.; Acciarri, M.; Lamanna, N.; Franzetti, A.; Zoia, L.; Bellini, M.; Berretti, E.; Lavacchi, A.; Santoro, C. Transforming Cigarette Wastes into Oxygen Reduction Reaction Electrocatalyst: Does Each Component Behave Differently? An Experimental Evaluation. *ChemElectrochem* **2024**, *11* (11), No. e202300725.
(50) Mecheri, B.; Ficca, V. C. A.; Costa de Oliveira, M. A.; D'Epifanio, A.; Placidi, E.; Arciprete, F.; Licoccia, S. Facile Synthesis of Graphene-Phthalocyanine Composites as Oxygen Reduction Electrocatalysts in Microbial Fuel Cells. *Appl. Catal., B* **2018**, *237*, 699−707.
(51) Ficca, V. C. A.; Santoro, C.; Placidi, E.; Arciprete, F.; Serov, A.; Atanassov, P.; Mecheri, B. Exchange Current Density as an Effective Descriptor of Poisoning of Active Sites in Platinum Group Metal-Free Electrocatalysts for Oxygen Reduction Reaction. *ACS Catal.* **2023**, *13* (4), 2162−2175.
(52) Ficca, V. C. A.; Sbroscia, M.; Stellino, E.; Rago, I.; Goto, F.; Majumdar, I.; Cavoto, G.; Pandolfi, F.; Calloni, A.; Lucotti, A.; Bussetti, G.; Placidi, E. Non-Chemical Route to PGM-Free via N+ Ion Implantation in Vertically Aligned Carbon Nanotubes. *Adv. Funct. Mater.* **2025**, *35* (4), 2413308.
(53) Crestini, C.; Lange, H.; Sette, M.; Argyropoulos, D. S. On the Structure of Softwood Kraft Lignin. *Green Chem* **2017**, *19* (17), 4104−4121.
(54) Sakai, K.; Kondo, T. Delignification in Peracetic Acid. II. Peraceric Acid Oxidation of Lignin Preparations. *Mokuzai Gakkaishi* **1966**, *12*, 310−315.
(55) Ishikawa, H. W.; Oki, T. Studies on the Oxidation Decomposition of Lignin. 2. Degradation by Sodium Peroxide of Aromatic Compounds Structurally Related to Softwood Lignin. *Japanese TAPPI* **1964**, *18*, 477−484.
(56) Krisnangkura, K.; Gold, M. H. Characterization of Guaiacyl Lignin Degraded by the White Rot Basidomycete Phanerochaete Chrysosporium. **1979**, *33*(5), 174−176. .
(57) Potthast, A.; Rosenau, T.; Chen, C.-L.; Gratzl, J. S. Selective Enzymic Oxidation of Aromatic Methyl Groups to Aldehydes. *J. Org. Chem.* **1995**, *60* (14), 4320−4321.
(58) Fabbrini, M.; Galli, C.; Gentili, P.; Macchitella, D. An Oxidation of Alcohols by Oxygen with the Enzyme Laccase and Mediation by TEMPO. *Tetrahedron Lett.* **2001**, *42* (43), 7551−7553.
(59) Fabbrini, M.; Galli, C.; Gentili, P. Comparing the Catalytic Efficiency of Some Mediators of Laccase. *J. Mol. Catal. B: Enzym.* **2002**, *16* (5), 231−240.
(60) Kawai, S.; Umezawa, T.; Higuchi, T. Degradation mechanisms of phenolic β-1 lignin substructure model compounds by laccase of Coriolus versicolor. *Arch. Biochem. Biophys.* **1988**, *262* (1), 99−110.
(61) Ikeda, R.; Sugihara, J.; Uyama, H.; Kobayashi, S. Enzymatic Oxidative Polymerization of 4-Hydroxybenzoic Acid Derivatives to Poly(Phenylene Oxide)s. *Polym. Int.* **1998**, *47* (3), 295−301.
(62) Tranchimand, S.; Tron, T.; Gaudin, C.; Iacazio, G. First Chemical Synthesis of Three Natural Depsides Involved in Flavonol Catabolism and Related to Quercetinase Catalysis. *Synth. Commun.* **2006**, *36* (5), 587−597.
(63) Colucci, G.; Gigli, M.; Sgarzi, M.; Rodrigues, A. E.; Crestini, C.; Barreiro, M. F. Modulation of Physicochemical and Antioxidant Properties of Pickering Emulsions Using Colloidal Lignin Particles Based on Kraft Softwood and Hardwood Acetone Fractions. *Sep. Purif. Technol.* **2024**, *347*, 127570.
(64) Sipponen, M. H.; Lange, H.; Ago, M.; Crestini, C. Understanding Lignin Aggregation Processes. A Case Study: Budesonide Entrapment and Stimuli Controlled Release from Lignin Nanoparticles. *ACS Sustainable Chem. Eng.* **2018**, *6* (7), 9342−9351.
(65) Sgarzi, M.; Gigli, M.; Babar, S.; Pajer, N.; Peroni, G.; Crestini, C.; Tverdokhleb, N.; Dianat, A.; Gutierrez, R.; Cuniberti, G. Supramolecular Interactions in Softwood Kraft Lignin Nanoparticles. *Faraday Discuss* **2026**, *263*, 123.

https://doi.org/10.1021/acssuschemeng.6c00142
ACS Sustainable Chem. Eng. 2026, 14, 8233−8243